Journal of Catalysis 260 (2008) 270–275

Contents lists available at ScienceDirect

Journal of Catalysis

www.elsevier.com/locate/jcat

Chemical and geometric effects of Ce and washcoat addition on catalytic partial oxidation of CH_4 on Rh probed by spatially resolved measurements

Alessandro Donazzi [a,b], Brian C. Michael [a], Lanny D. Schmidt [a,*]

[a] Department of Chemical Engineering and Materials Science, University of Minnesota, 421 Washington Avenue SE, Minneapolis, MN 55455, USA
[b] Laboratorio di Catalisi e Processi Catalitici, Dipartimento di Energia, Politecnico di Milano, Piazza Leonardo da Vinci 32, 20133 Milano, Italy

ARTICLE INFO

Article history:
Received 1 August 2008
Revised 24 September 2008
Accepted 30 September 2008
Available online 22 October 2008

Keywords:
Methane
Catalytic partial oxidation
Steam reforming
Spatial profiles
Rh
Ce
Thermodynamics

ABSTRACT

Using a spatially resolved sampling technique, the catalytic partial oxidation of CH_4 to synthesis gas was investigated over 80 ppi α-Al_2O_3 foams coated with three catalytic formulations: 5 wt% Rh, 5 wt% Rh/2 wt% γ-Al_2O_3 washcoat and 5 wt% Rh–2 wt% Ce/2 wt% γ-Al_2O_3 washcoat. Experiments were performed at atmospheric pressure and ~8 millisecond contact time, with 20% v/v CH_4 and C/O ratio equal to 1. Data show that the length of the oxidative zone (~2 mm) is unaffected by the composition of the catalyst. The addition of γ-Al_2O_3 washcoat to Rh coated monoliths allows the reaction to reach adiabatic equilibrium by increasing the rates of steam reforming and water gas shift. Additionally, both the maximum and the gradients in the temperature profiles decrease significantly with the addition of washcoat. Data collected on Rh–Ce/washcoat show that the adiabatic equilibrium composition is reached through a different kinetic route: the consumption of CH_4 becomes slower, the production of CO_2 exhibits a maximum, and the production of H_2O is drastically moderated, suggesting that Ce has an active role in the CPO reaction kinetics. The features presented could be detected exclusively with spatially resolved measurements.

1. Introduction

The catalytic partial oxidation (CPO) of CH_4 is one of the most attractive technologies for the production of syngas in small- to medium-scale applications. CPO can be conducted at millisecond contact times, under autothermal conditions to yield high selectivities to syngas [1]. These features allow for the design of simple and compact reactors, with fast dynamic responses and low heat capacity, which are ideal for mobile and stationary production of syngas. In order to achieve such a high flexibility of operation, CPO reactors operate under extremely high gradients in temperature and composition with complex fluid and kinetic patterns, where mass and heat transfer are coupled with surface processes.

The mechanism of methane CPO [Eq. (1)] is still debated. Depending on the formulation of the catalyst, the nature of the support, and the operating conditions adopted, different distribution of products have been observed and different pathways have been proposed [2]. Detailed schemes are used to explain the process in terms of elementary steps [3,4]. Nonetheless, the mechanism can be described globally in terms of an initial exothermic oxidative process, either direct partial oxidation [Eq. (1)] or total combustion [Eq. (2)], followed by endothermic steam reforming [SR, Eq. (3)] and water gas shift [WGS, Eq. (4)]. Some authors include CO_2-reforming [Eq. (5)] in the mechanism.

$$CH_4 + (1/2)O_2 \rightarrow CO + 2H_2, \qquad \Delta H_r^0 = -36\ \text{kJ mol}^{-1}, \tag{1}$$

$$CH_4 + 2O_2 \rightarrow CO_2 + 2H_2O, \qquad \Delta H_r^0 = -803\ \text{kJ mol}^{-1}, \tag{2}$$

$$CH_4 + H_2O \leftrightarrow 3H_2 + CO, \qquad \Delta H_r^0 = +206\ \text{kJ mol}^{-1}, \tag{3}$$

$$H_2O + CO \leftrightarrow H_2 + CO_2, \qquad \Delta H_r^0 = -41\ \text{kJ mol}^{-1}, \tag{4}$$

$$CH_4 + CO_2 \leftrightarrow 2H_2 + 2CO, \qquad \Delta H_r^0 = +247\ \text{kJ mol}^{-1}. \tag{5}$$

In general, it is agreed upon that Group VIII noble metals give the best performance, with Rh providing the highest selectivity to H_2, carbon-free operation, and better stability against volatilization [5]. Due to its high cost, Rh must be utilized as efficiently as possible in order to make the technology economical. Key features of the reactor design thus involve optimization of the catalyst in terms of metal loading, dispersion, and thermal management. Some common approaches to accomplish this are to modify the support with the addition of washcoat, or to add a promoter such as Ce in order to promote or suppress certain kinetic routes. The addition of washcoat increases the surface area of the support and the metal dispersion and inhibits the sintering of the catalyst [6]. On noble metals, Ce is reported to increase the activity of WGS [Eq. (4)] [7–10] and to catalyze the direct partial oxidation of CH_4 [Eq. (1)] [11]. Furthermore, Ce can also stabilize the alumina support [12] and prevent sintering of the catalyst [13]. Experimental

* Corresponding author.
E-mail address: schmi001@umn.edu (L.D. Schmidt).

0021-9517/$ – see front matter
doi:10.1016/j.jcat.2008.09.028

data on the effect of these modifications is highly valuable since modeling them is a difficult task. Recently, Horn et al. [14,15] developed a technique to acquire measurements within a reactor and demonstrated that spatially resolved measurements are a powerful tool for understanding the CPO process. The present study shows that, although the benefits of Ce and washcoat are seen in integral data, the extent of their individual effect is more complex and can be observed only through spatially resolved measurements.

2. Experimental

2.1. Catalysts preparation

80 ppi α-Al_2O_3 reticulated foam monoliths (11 mm long, 17 mm diameter) were used as supports. The monoliths were drilled axially with an ultrasonic drill to form a hole of 770 μm diameter. The catalyst samples were prepared using the incipient wetness technique. Three catalytic formulations were compared: 5 wt% Rh (hereafter referred as Rh), 5 wt% Rh/2 wt% γ-Al_2O_3 washcoat (Rh/wc) and 5 wt% Rh–2 wt% Ce/2 wt% γ-Al_2O_3 washcoat (Rh–Ce/wc). Washcoat was applied as an aqueous slurry of γ-Al_2O_3 (3 μm powder, SA 80–120 m^2/g) after which the samples were calcined at 600 °C for 6 h. Rh and Ce were deposited as aqueous solutions of $Rh(NO_3)_3$ and $Ce(NO_3)_3$, respectively. In the case of Rh–Ce samples, Ce and Rh were deposited simultaneously. After the application of the metals, the impregnated monoliths were calcined in air at 600 °C for 6 h.

2.2. Apparatus and operating conditions

The reactor consisted of a quartz tube (18 mm I.D.) into which the catalytic monolith was placed along with blank monoliths fore and aft, which acted as shields to prevent axial heat loss. The monoliths were wrapped in aluminosilicate paper to prevent bypass, and the exterior reactor body was insulated to avoid radial heat losses. A deactivated fused silica capillary (550 μm O.D.) with a ∼200 μm side orifice placed ∼35 mm from the sealed tip was used for sampling gases. The capillary was inserted through the drilled holes of the monoliths, forming an annulus of 110 μm, and attached to a microvolume tee mounted on a linear translation stage. Two heated stainless steel capillaries were attached to the tee, one connected to the leak valve of a quadrupole mass spectrometer (QMS, UTI 100C), the other to the sample loop of a gas chromatograph (GC, HP5890 equipped with a HayeSep D packed column and a TCD). Gas samples were drawn through the orifice to both the high pressure side of the QMS leak valve, and to the return of the GC line by a vacuum pump. Further details on the sampling apparatus are given in [15].

An optical pyrometer (Mikron MI-GA 5-LO) and a thermocouple (Inconel clad K-type, 0.254 mm diameter) were used to measure the temperature. A quartz optical fiber with 45° polished tip was used as probe for the pyrometer, which yielded an accuracy of ±10 °C. Temperature profiles were acquired by inserting the thermocouple or the optical fiber into the capillary. The pyrometer readings are assumed to be representative of the surface temperature, while the thermocouple readings were considered representative of the gas temperature [14].

All the experiments shown here were performed at atmospheric pressure, with a flow rate of 5 SLPM, C/O ratio of 1, and with 20% v/v CH_4. Gases were preheated to 150 °C. Ar was used as an inert diluent and internal standard for GC and QMS. H_2O was calculated by closing the atomic balance on O, while the C and H balances closed to within ±3%. All data presented were replicated on three different monoliths. Each catalyst was run for up to 60 h without any sign of deactivation.

The reacting mixture was slightly diluted compared to that commonly adopted in the literature, which simulates the autothermal CPO of CH_4 in air [14,15]. This dilution was chosen in order to widen the experimental window where the observed effects are sufficiently distant from the thermodynamic equilibrium limits. The heat dissipated was negligible compared to the enthalpy supplied to the reactor, and the adiabatic condition was closely approached.

3. Results

Table 1 lists CH_4 conversion, H_2 and CO selectivities and the outlet temperature of the three catalysts, compared to the same values calculated at the adiabatic equilibrium (constant pressure and enthalpy, $T_{IN} = 150$ °C). It can be seen that Rh/wc and Rh–Ce/wc reach the adiabatic equilibrium within the experimental error, whereas Rh has lower conversion of CH_4 and selectivity to H_2 as well as a 53 °C higher outlet temperature than equilibrium predicts.

Fig. 1 shows the spatial profiles collected on the three catalysts. No evidence of activity is observed in the inlet monolith ($-4 < z < 0$) or in the outlet monolith ($11 < z < 14$), in accord with the absence of homogeneous contributions previously reported under comparable operating conditions [14,15].

The profiles for CH_4 and O_2 are presented in Fig. 1a. In all the samples, the length of the oxidation zone (the zone in the catalyst where O_2 conversion takes place) is almost unchanged, moving from 1.8 mm for Rh to 2.3 mm over Rh/wc and Rh–Ce/wc. This variability, which is confined to the last part of the oxidation zone, can be ascribed to the differences in the fine internal structures of each of the foams used (pore blockage, bypasses). The equivalence of the oxidation curves regardless of the catalyst composition is in agreement with the presence of strong O_2 mass transfer limitations in the first part of the monolith where highly exothermic processes are localized.

In the oxidation zone, CH_4 is consumed with similar shape for all three catalysts, but with different rates that increase in the sequence: Rh < Rh–Ce/wc < Rh/wc. In the reforming zone (where gas phase O_2 is absent and CH_4 is converted via reforming reactions) the CH_4 behavior is distinct for each of the samples. For Rh/wc, the consumption of CH_4 proceeds at a rate nearly equal to that in the oxidation zone and terminates abruptly at its final value within ∼3 mm of the catalyst entrance. The reforming activity of Rh occurs much slower than for Rh/wc: CH_4 is consumed throughout the entire reactor and does not equilibrate by the outlet. Again, Rh–Ce/wc exhibits intermediate behavior but still equilibrates the products.

Panels (b) and (c) in Fig. 1 show the concentration profiles of the products, H_2, H_2O, CO and CO_2. It is useful to refer to Fig. 2, in the description that follows: the bar chart is a comparison of the compositions measured at the end of the oxidation zone (Z_{ox}) and at the outlet of the reactor for each catalyst analyzed.

Table 1
Reactor outlet conversions, selectivities and temperature (pyrometer reading) for the three catalyst analyzed compared to the adiabatic equilibrium values calculate at constant P and H for $T_{IN} = 150$ °C.

	Rh	Rh/wc	Rh–Ce/wc	Adiabatic equilibrium
X CH_4 (%)	68.8%	78.2%	79.8%	80.3%
S CO (%)	88.1%	88.9%	85.9%	87.7%
S H_2 (%)	84.6%	91.0%	92.2%	93.4%
S H_2O (%)	15.4%	9.0%	7.8%	6.6%
S CO_2 (%)	11.9%	11.1%	14.1%	12.3%
T_{out} (°C)	709	639	640	656

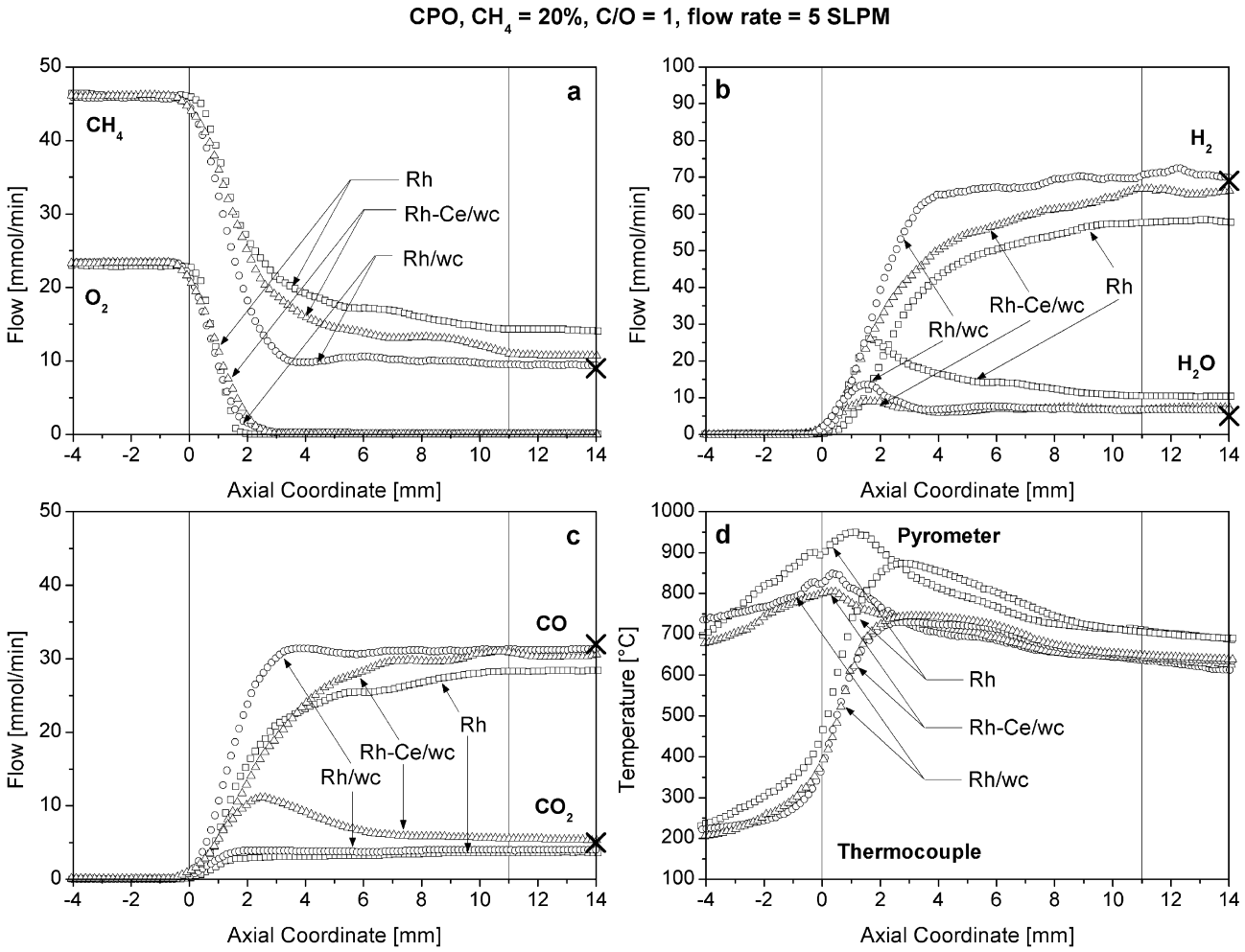

Fig. 1. Composition and temperature profiles for CPO on the three catalysts analyzed. $CH_4/O_2/Ar = 20/10/70\%$ v/v. Flow = 5 SLPM. Symbols: 5 wt% Rh/α-Al_2O_3 (□); 5 wt% Rh/2 wt% γ-Al_2O_3/α-Al_2O_3 (○); 5 wt% Rh–2 wt% Ce/2% γ-Al_2O_3/α-Al_2O_3 (△); equilibrium (×). Panel (a) CH_4 and O_2 molar flow. Panel (b) H_2 and H_2O molar flow. Panel (c) CO_2 and CO molar flow. Panel (d) pyrometer and thermocouple profiles.

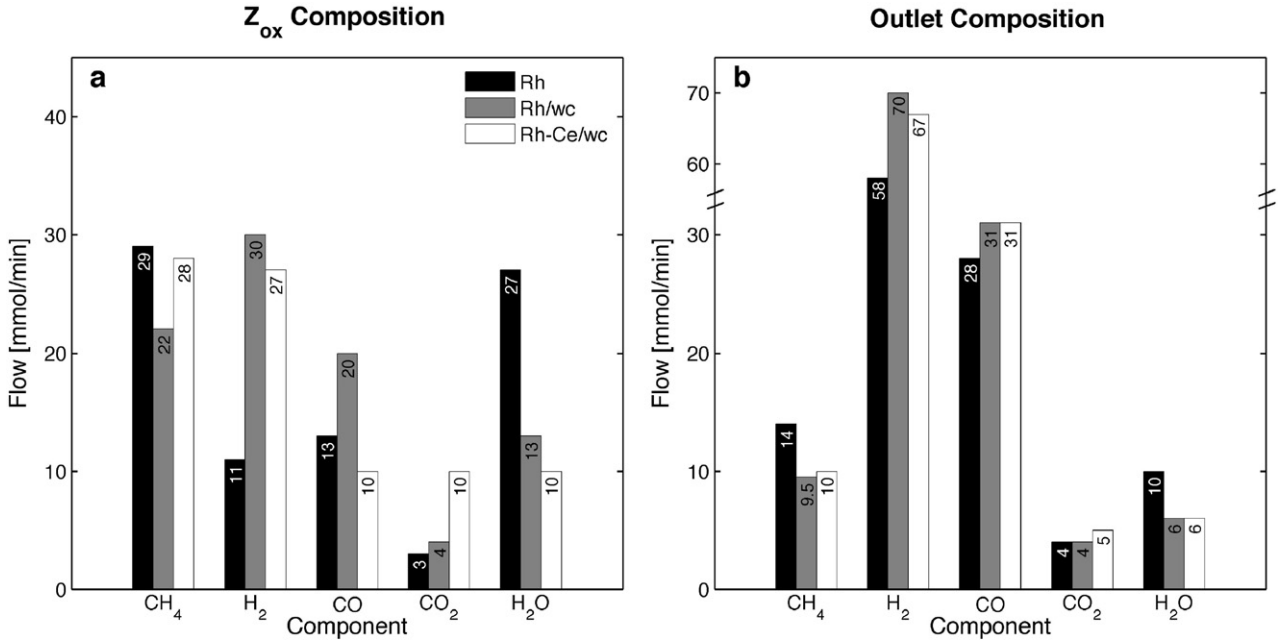

Fig. 2. Comparison among the molar flows of reactants and products measured at the end of the oxidation zone [Z_{ox}, panel (a)] and of the monolith [panel (b)] for the three catalysts analyzed.

Syngas production qualitatively follows the trend of the CH_4 conversion curves, slowly growing with Rh and Rh–Ce/wc samples, and quickly leveling at the equilibrium values in the case of Rh/wc.

The Rh sample displays the lowest formation rate of syngas. Rh/wc and Rh–Ce/wc have almost equal H_2 production in the oxidation zone while, in the reforming zone, the rate of formation appears to decrease with the addition of Ce. In the oxidation zone, Rh–Ce/wc gives almost half of the production of CO as Rh/wc. After ∼4 mm, the CO formation on Rh–Ce/wc proceeds to equilibrium, in line with CH_4 conversion.

The most remarkable contrasts are observed in CO_2 and H_2O concentration profiles. The evolution of H_2O is that typical of a reaction intermediate species: it passes through a maximum near the end of the oxidation zone and is followed by a decrease toward equilibrium. The peak value of H_2O, as well as its axial concentration, decreases in the sequence: Rh > Rh/wc > Rh–Ce/wc.

The differences in concentration profiles of CO_2 are even more striking. On Rh and Rh/wc, CO_2 production takes place primarily in the oxidation zone and remains constant throughout the rest of the catalyst, in line with the behavior of a primary product that does not react further. On Rh–Ce/wc, CO_2 follows a significantly different trend: first, it goes through a maximum at 2.6 mm followed by a progressive consumption to the final value, in line with the characteristic evolution of intermediate products. Furthermore, in the oxidation zone, CO_2 and CO are produced with a ratio of 1:1, and their formation curves completely overlap. In contrast, the production of CO is always greater than that of CO_2 over non-Ce catalysts.

The temperature profiles are shown in Fig. 1d. The pyrometer readings show that washcoated catalysts operate at lower temperatures and reach the adiabatic equilibrium temperature at the outlet (Table 1). The addition of the washcoat causes a pronounced decrease in the gradients as well as a moderation of the maxima, which drop from ∼950 °C on Rh to ∼850 °C on Rh/wc and ∼800 °C on Rh–Ce/wc. Furthermore, the maxima move upstream, going from 1.1 mm (Rh) to 0.3 mm (Rh/wc, Rh–Ce/wc). Similar to the pyrometer, thermocouple profiles have maxima that occur at ∼2.9 mm regardless of the catalyst composition. Before reaching the maxima, the curves display a steep gradient (150 °C/mm on Rh, 120 °C/mm on Rh/wc and Rh–Ce/wc) followed by a slow decrease, with temperatures that locally overtake the pyrometer readings. In all cases, the thermocouple readings match the pyrometer readings in the last part of the monolith, indicating gas and surface thermal equilibration.

A useful comparison of the catalysts performance can be done on the basis of the approach to equilibrium according to two independent reactions, namely steam reforming [Eq. (3)] and WGS [Eq. (4)]. The curves presented in Fig. 3 are calculated from the data within the reactor according to:

$$\left(\frac{K_{EXP}}{K_{EQ}}\right)_{SR} = \frac{P_{H_2}^3 P_{CO}}{P_{CH_4} P_{H_2O}} \cdot \frac{1}{K_{eq,SR}}, \tag{6}$$

$$\left(\frac{K_{EXP}}{K_{EQ}}\right)_{WGS} = \frac{P_{H_2} P_{CO_2}}{P_{CO} P_{H_2O}} \cdot \frac{1}{K_{eq,WGS}}. \tag{7}$$

In Eqs. (6) and (7), $K_{EQ,SR}$ and $K_{EQ,WGS}$ are the equilibrium constants calculated with the temperature measured by the pyrometer. The P_i are partial pressures of species i. It can be seen that the addition of the washcoat brings steam reforming closer to the local equilibrium, however equilibrium is only reached at the outlet. With the addition of Ce, WGS is equilibrated.

4. Discussion

4.1. Effect of the washcoat over Rh based catalysts

On the Rh sample, the spatial profiles show that the reaction is limited by mass transfer in the oxidation zone; in the reforming zone, the CH_4 consumption by steam reforming is too slow to go to completion. This causes the catalyst to operate far from thermodynamic equilibrium, and results in reduced conversion of CH_4 and selectivity to syngas. The lack of endothermic chemistry causes a 53 °C higher outlet temperature than equilibrium (Table 1).

The addition of γ-Al_2O_3 washcoat allows the mixture to reach adiabatic equilibrium at the outlet. Moreover, the K_{EXP}/K_{EQ} ratios calculated along the axis for steam reforming (Fig. 3a) and WGS (Fig. 3b) increase by a factor of one hundred and ten, respectively. The composition profiles reveal that the chemistry is confined to a small fraction of the monolith (∼30%) where the curves continue with the same trend even outside the oxidation zone. The catalyst operates at lower temperatures with lower gradients, the temperature range going from ∼250 °C on the non-washcoated sample to ∼160 °C on the washcoated one.

As reported in [6] on the basis of SEM and EDS micrographs taken on similar Rh-coated 80 ppi α-Al_2O_3 foams, the addition of a washcoat of 3 μm γ-Al_2O_3 particles has two main effects: (1) it increases the surface area of the support and (2) it keeps the metal particles dispersed by reducing sintering. These modifications are purely geometric. In this way, the addition of washcoat increases the number of sites available for catalysis, consequently increasing the overall reaction rates of the main routes to equilibrium in the reforming section, steam reforming and WGS. Indeed, on Rh/Al_2O_3 catalysts, while WGS is known to be surface insensitive [10], steam reforming turnover frequency increases upon increasing the dispersion of the metal [16].

The evidence presented here suggests that, in the case of Rh/wc, the increase in the metal surface area makes the reaction rates so high that the entire process likely becomes limited by transport of reactants. Since all the chemistry occurs in a shorter portion of the monolith, the effects of the endothermic steam reforming and of the exothermic oxidation overlap, and the hot spot drops and moves upstream.

4.2. Effect of Ce addition over washcoated catalysts

Given that washcoated catalysts reach the thermodynamic equilibrium regardless of the composition (Table 1), the most striking aspect of the comparison between Rh–Ce/wc and Rh/wc is that the same final state is reached by two distinct evolutions of the products (Fig. 1).

In the oxidation zone, the conversion of CH_4 and the distribution of the products are different for the two catalysts. Since the consumption rate of O_2 is identical due to mass transfer limitations, the chemistry on the surface of Rh–Ce/wc must be different from that of Rh/wc. Using data from Fig. 2a, the following stoichiometric equations can be written for the end of the oxidation zone:

Rh/wc:

$$CH_4 + 0.9O_2 \rightarrow 1.4H_2 + 0.8CO + 0.6H_2O + 0.2CO_2,$$
$$\Delta H_r^0 = -231\ \text{kJ mol}^{-1}, \tag{8}$$

Rh–Ce/wc:

$$CH_4 + 1.0O_2 \rightarrow 1.5H_2 + 0.5CO + 0.5H_2O + 0.5CO_2,$$
$$\Delta H_r^0 = -306\ \text{kJ mol}^{-1}. \tag{9}$$

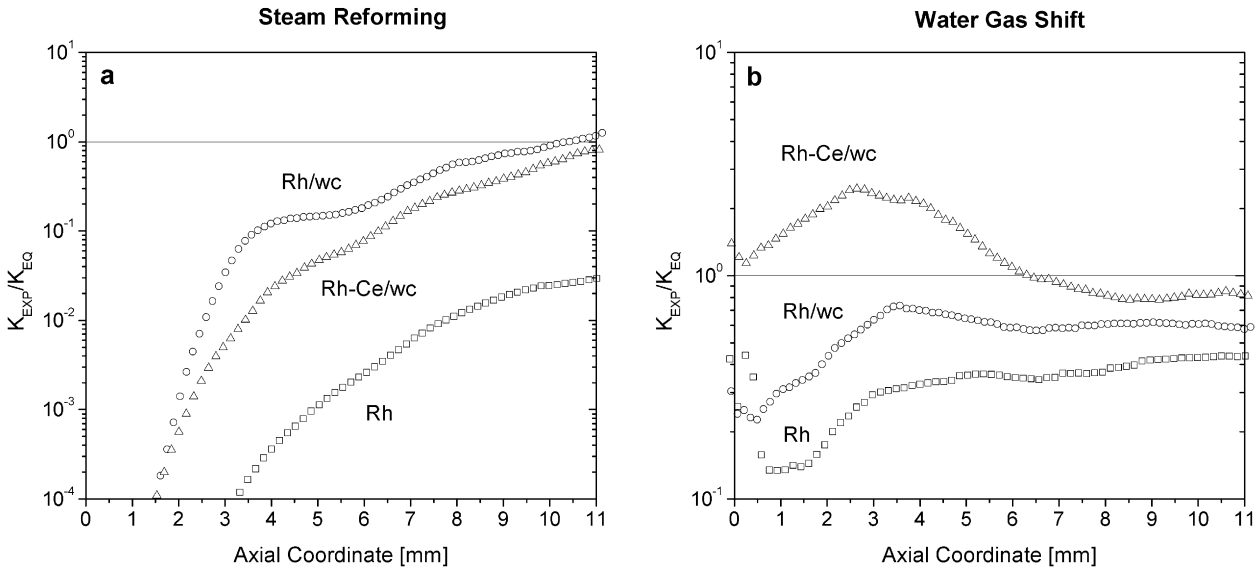

Fig. 3. K_P to K_{EQ} ratio for steam reforming [panel (a)] and WGS [panel (b)]. $CH_4/O_2/Ar = 20/10/70\%$ v/v. Flow = 5 SLPM. Symbols: 5 wt% Rh α-Al_2O_3 (□); 5 wt% Rh/2 wt% γ-Al_2O_3/α-Al_2O_3 (○); 5 wt% Rh–2 wt% Ce/2% γ-Al_2O_3/α-Al_2O_3 (Δ). Calculations are based on pyrometer readings.

The two catalysts form approximately the same amount of H_2 per mol of CH_4 consumed, but Rh–Ce/wc produces more than twice as much CO_2, at the expenses of CO. CO_2 and CO are produced with the same rate, thus indicating that they are parallel products.

In the reforming section, while Rh/wc retains high rates of reaction, Rh–Ce/wc shows a slow trend in the consumption of CH_4 and in the formation of syngas. Most importantly, the CO_2 produced in the oxidation zone is progressively consumed to its final value, giving rise to a peak that is absent in the other profile and whose position is shifted downstream of the peak in H_2O and pyrometer maxima.

Clearly this behavior indicates that Ce has an active role in the chemistry of CPO of CH_4, rather than just physically stabilizing the surface area of the washcoat [12] and preventing the sintering of Rh particles [13]. The addition of Ce likely changes the mechanistic pattern of the process, either by introducing new routes or by selectively promoting the existing ones. Along with this property, the presence of Ce modifies the nature of the active sites, thus changing the effect of the washcoat on the rates of reaction. As a consequence, a rigorous kinetic mechanism cannot be extracted on the basis of this data alone, but the insight that they provide is sufficient to elucidate the most important features of the process.

In the oxidation zone, although the production of H_2 is almost equal over the two catalysts, Rh–Ce/wc displays lower conversion of CH_4. It can be speculated that WGS provides an extra route for H_2 production. The considerable increase in WGS activity due to the addition of Ce to noble metal catalysts is a widely documented subject in the literature [7–9] and agrees well with the evidence of higher production of CO_2 and lower production of CO and H_2O.

In the reforming zone, as clearly shown in the plot of K_{EXP}/K_{EQ} of Fig. 3b, WGS remains close to equilibrium. This means that the product distribution expected from WGS is observed and is a consequence of the temperatures dictated by the highly exothermic and endothermic conversion routes of CH_4. Fig. 3a shows also that the thermodynamic driving force for steam reforming is almost unaltered on the washcoated catalysts. The apparent stoichiometry of CO_2-reforming can thus be explained by the combination of steam reforming and quasi-equilibrated reverse WGS (RWGS).

It has been reported for various noble metals and supports [17–19] that a cycle of steam reforming and RWGS is favored over direct CO_2-reforming in the presence of H_2O and O_2. Furthermore, the ability of Ce to absorb and activate CO_2 is also documented [20] and is in line with the possibility of a high RWGS activity.

Together with a chemical role, a significant morphological role of Ce cannot be excluded. Fig. 1 shows indeed that the steam reforming activity is lower for Rh–Ce/wc than for Rh/wc. This observation, which apparently conflicts with the promotion of steam reforming induced by Ce [21], could be explained on the basis of a loss of surface metal area either by decoration of Rh particles by partially reduced Ce oxides or by the significant inhomogeneity of the surface due to the procedure used to prepare the catalyst. Given the importance of metal–ceria interactions [22] in determining the final activity of the catalyst, further characterization is needed to access the nature of the effect.

5. Conclusion

Results presented in this work focus on the effect of adding γ-Al_2O_3 washcoat and Ce to 5 wt% Rh-coated 80 ppi α-Al_2O_3 foams on the partial oxidation of CH_4. Activity tests were performed at millisecond contact times under autothermal conditions, with 20% v/v CH_4 and C/O ratio equal to 1. A spatially resolved sampling technique was applied to measure temperature and concentration profiles. From the data it can be concluded that:

(1) The addition of the washcoat increases the rate of reaction such that the volume of the monolith involved in the process reduces to a fraction (∼30%) of that needed in the absence of washcoat. Temperature gradients significantly decrease due to the overlap of the oxidation and the reforming zones. Under the present operating conditions, the washcoat enables equilibration by increasing the rate of steam reforming and WGS.
(2) The addition of Ce changes the evolution of the CPO process as evidenced by the maximum in the CO_2 concentration profile. The spatial profiles confirm the synergetic interaction between Rh and Ce, but the complexity of the phenomena prohibits any conclusive statement. Nonetheless, the apparent stoichiometry of CO_2 reforming can be explained on the basis of quasi-equilibrated WGS (enhanced by the addition of Ce) and steam reforming.
(3) Spatial profiles supply highly valuable information in the comparison of the activity of different catalysts. As in the case of Ce addition, they emphasize aspects that integral data alone

cannot capture. Attempts to model CPO on Rh/wc would require modification to the active site concentration, whereas attempts to model CPO on Rh–Ce/wc would most likely require modification to the rate constants of steps involved in WGS.

References

[1] D.A. Hickman, L.D. Schmidt, J. Catal. 138 (1992) 267.
[2] A.P.E. York, T. Xiao, M.L.H. Green, J.B. Claridge, Catal. Rev. Sci. Eng. 49 (2007) 511.
[3] R. Schwiedernoch, S. Tischer, C. Correa, O. Deutschmann, Chem. Eng. Sci. 58 (2003) 633.
[4] A.B. Mhadeshwar, D.G. Vlachos, J. Phys. Chem. B 109 (2005) 16819.
[5] P. Aghalayam, Y.K. Park, D.G. Vlachos, Catalysis 15 (2000) 98.
[6] N.J. Degenstein, R. Subramanian, L.D. Schmidt, Appl. Catal. A Gen. 305 (2006) 146.
[7] C. Wheeler, A. Jhalani, E.J. Klein, S. Tummala, L.D. Schmidt, J. Catal. 223 (2004) 191.
[8] J. Barbier, D. Duprez, Appl. Catal. B Environ. 3 (1993) 61.
[9] T. Bunluesin, R.J. Gorte, G.W. Graham, Appl. Catal. B Environ. 15 (1998) 107.
[10] D.C. Grenoble, M.M. Estadt, D.F. Ollis, J. Catal. 67 (1981) 90.
[11] K. Otsuka, Y. Wang, E. Sunada, I. Yamanaka, J. Catal. 175 (1998) 152.
[12] J.S. Church, N.W. Cant, D.L. Trimm, Appl. Catal. A Gen. 101 (1993) 105.
[13] J.M. Schwartz, L.D. Schmidt, J. Catal. 138 (1992) 283.
[14] R. Horn, K.A. Williams, N.J. Degenstein, A. Bitsch-Larsen, D. Dalle Nogare, S.A. Tupy, L.D. Schmidt, J. Catal. 249 (2007) 378.
[15] R. Horn, N.J. Degenstein, K.A. Williams, L.D. Schmidt, Catal. Lett. 110 (2006) 169.
[16] J. Wei, E. Iglesia, J. Catal. 225 (2004) 116.
[17] M.C.J. Bradford, M.A. Vannice, Appl. Catal. A 142 (1996) 73.
[18] J.R. Rostrup-Nielsen, J.H. Bak Hansen, J. Catal. 144 (1993) 38.
[19] A. Donazzi, A. Beretta, G. Groppi, P. Forzatti, J. Catal. 225 (2008) 241.
[20] C. de Leitenburg, A. Trovarelli, J. Kaspar, J. Catal. 166 (1997) 98.
[21] A. Trovarelli, Catal. Rev. Sci. Eng. 38 (1996) 439.
[22] V.M. Gonzalez-DelaCruz, J.P. Holgado, R. Pereñiguez, A. Caballero, J. Catal. 257 (2008) 307.